

Aerosol-Assisted Chemical Vapor Deposition (AACVD) Technique of SrTiO₃: B Thin Films and Study the Structural and Optical Properties and Hall Effect Measurements

Yahya M. Abdul-Hussein^{1*}, Randa K. Hussain², Mohammed K. Khalaf¹

¹Materials Researches Directorate, Ministry of higher Education and Scientific Research, Science and Technology, Baghdad, IRAQ.

²Department of Physics, College of Sciences, Mustansiriyah University, Baghdad, IRAQ.

*Correspondent contact: Yahyamus1975@gmail.com

Article Info

Received
26/06/2022

Accepted
06/09/2022

Published
30/12/2022

ABSTRACT

Aerosol-assisted chemical vapor deposition (AACVD) technique is very precise and implemented for the fabrication of structured SrTiO₃ and Sr_{1-x}B_xTiO₃ thin films at doping ratio (x = 2, 4, 6 and 8) % at temperature 400 °C on a glass substrate. The X-Ray Diffraction (XRD) patterns illustrated that the SrTiO₃ and Sr_{1-x}B_xTiO₃ thin films have a polycrystalline nature and cubic structure, the detailed characterization of the films by X-ray diffraction (XRD), the Surface Morphology studied by using (AFM) and (SEM). Have been noticed from AFM measurement the Roughness and RMS were increased with increases doping ratio. The optical properties of SrTiO₃ and Sr_{1-x}B_xTiO₃ thin films have been studied at doping ratio (x = 2, 4, 6 and 8) % at range (300-900) nm. The transmittance spectrum is characterized by the opposite behavior of the absorbance spectrum. The transmittance generally increases with an increased in the wavelength of radiation, at wavelengths with low energies while the absorbance decreased slowly at the spectrum range (300-900) nm i.e. in the visible region. The band gap (E_g) is decreased at (3.2 - 2.5) eV which indicates that the doping process has led to the emergence of localized levels in the region confined by the valence and conduction bands, led to a reduction in the photon energy required for direct electronic transitions to occur. Found the carrier's concentration charge are holes of Sr_{1-x}B_xTiO₃ thin films at doping ratio (x = 2, 4, 6 and 8) %. Many properties can be improved by adding impurities such as Boron (B) to the SrTiO₃, which can be used in solar cells, electronic industries or thermoelectric generators by controlling the optical or structural properties of the material by controlling the materials and percentages of impurity, or through heat treatment of the material, such as annealing, for example or exposure to different temperatures.

KEYWORDS: AACVD; Hall effect; optical properties; SrTiO₃ /Sr_{1-x}B_xTiO₃; structural properties.

الخلاصة

يتم تنفيذ تقنية ترسيب البخار الكيميائي بمساعدة الرذاذ الجوي (AACVD) بدقة كبيرة لتحضير الأغشية الرقيقة SrTiO₃ و Sr_{1-x}B_xTiO₃ بنسبة المنشطات (% (x=2, 4, 6, 8) عند درجة حرارة 400 درجة مئوية على ركائز زجاجية. أوضحت أنماط حيود الأشعة السينية (XRD) أن الأغشية الرقيقة SrTiO₃ و Sr_{1-x}B_xTiO₃ لها طبيعة متعددة الكريستالات وهيكل مكعب، والوصف التفصيلي للأغشية عن طريق حيود الأشعة السينية (XRD)، ودراسة التشكل السطحي باستخدام (AFM). (SEM). لوحظ من قياس AFM زيادة الخشونة و RMS مع زيادة نسبة المنشطات. تمت دراسة الخواص البصرية للأغشية الرقيقة SrTiO₃ و Sr_{1-x}B_xTiO₃ بنسبة المنشطات (% (x=2, 4, 6, 8) بمعدل (300-900) نانومتر. يتميز طيف النفاذية بالسلوك المعاكس لطيف الامتصاصية. تزداد النفاذية بشكل عام مع زيادة الطول الموجي للإشعاع، عند الأطوال الموجية ذات الطاقات المنخفضة بينما ينخفض الامتصاص ببطء عند معدل الطيف (300-900) نانومتر، أي في المنطقة المرئية. يتم تقليل فجوة النطاق على سبيل المثال عند (3.2-2.5) eV مما يشير إلى أن عملية المنشطات أدت إلى ظهور مستويات محلية في المنطقة المحصورة بواسطة نطاقات التكافؤ والتوصيل، مما أدى إلى انخفاض طاقة الفوتون المطلوبة للإلكترونات المباشرة حدوث انتقالات. تم العثور على شحنة تركيز الحاملات عبارة عن ثقب من الأغشية الرقيقة Sr_{1-x}B_xTiO₃ بنسبة المنشطات (% (x=2, 4, 6, 8). يمكن تحسين العديد من الخصائص عن طريق إضافة بعض أنواع الشوائب مثل البورون (B) إلى SrTiO₃، والتي يمكن استخدامها في الخلايا الشمسية أو الصناعات الإلكترونية أو المولدات الكهروحرارية عن طريق التحكم

في الخصائص البصرية أو الهيكلية للمادة عن طريق التحكم في المواد والنسب المئوية من الشوائب، أو من خلال المعالجة الحرارية للمادة، مثل التلدين، على سبيل المثال أو التعرض لدرجات حرارة مختلفة.

INTRODUCTION

Strontium titanate (SrTiO₃) is a perovskite material that has very important physical properties and depends on its chemical composition. SrTiO₃ is semiconductor n-type with an indirect wide bandgap (3.2 eV). The physical properties also depend on some factors such as electric field, pressure, temperature, etc. as it has a high permittivity at room temperature, it has phase transitions from a semi-electric compound to a ferroelectric compound SrTiO₃ can be superconducting at low temperatures and can be n-type charge carriers when doped with some materials such as niobium or lanthanum or samarium [1, 2]. The thin-film SrTiO₃ has the application of resistive random access memory (ReRAM) due to its possession of resistive switching behavior. This perovskite compound under low oxygen conditions has high chemical stability and changes into a highly conductive n-type material either by adding impurities or by reducing, the material that has a high dielectric constant has important applications, especially in wireless communication technology [3–5]. SrTiO₃ has high dielectric permittivity, low microwave loss, low leakage current, and high breakdown strength, so it has wide applications in the electronic ceramic industries and microwaves [6]. Due to the distinct optical properties possessed by strontium oxide titanate with perovskite (SrTiO₃), for example, we find that the optical absorption is affected by several factors, including the ratio of defects and impurities and the grain boundaries of the surface [7, 8]. When studying the optical features of SrTiO₃ thin films on Si, it was found that due to the growing effect of the amorphous interlayer between the SrTiO₃ film and the Si substrate, the refractive index decreases below the bandgap with lessening thickness [9]. Have been fabricated this films by many operations such as molecular beam epitaxial (MBE), Metal-Organic Chemical Vapor Deposition (MOCVD), pulsed laser deposition (PLD), ion beam sputtering, divergent magnetic field type electron-cyclotron-resonance (ECR) plasma sputtering and RF magnetron sputtering [10]. SrTiO₃ has been used in the optical field as grain boundary barrier layer capacitors, laser frequency multiplexing, catalytic doping, waveguides [11, 12]. In this paper, we have

investigated the effects of doping ratio on the structural, properties and Hall effect measurement of SrTiO₃ thin films synthesis on glass substrates by the AACVD technique. the perovskite material SrTiO₃ has electrical, optical, and structural properties so that it is important in many applications such as the field of sensors, photodetectors, and electrothermal applications.

MATERIALS AND METHODS

In the following process steps:

Using aerosol-assisted chemical vapor deposition (AACVD) method to deposition Strontium titanate SrTiO₃ and Sr_{1-x}B_xTiO₃ thin films were carried out in the process steps for each of these are as follows: Strontium chloride (SrCl₂) was dissolved by distilled water and Titanium trichloride (TiCl₃) was dissolved by ethanol, mixed, and add Boric acid (H₃BO₃) when dissolved by distilled water at preper Sr_{1-x}B_xTiO₃ thin film In the case of doping with Boron and put the solution on the magnetic stirrer at 15 minutes. When solution became homogeneous and then deposited by (AACVD) method on the glass substrates that putted on the hot plate at a fixed temperature at 400 °C to prepare SrTiO₃ thin film. The (XRD) instrument are of type (Shimadzu 6000) made in Japan, with the following specifications:

Target: Cu K α

Wavelength: 1.5406 Å

Voltage: 40 kV

Current: 30 mA

The Atomic Force Microscopy (AFM) (angstrom advance INC, SPM, AA-3000) made in USA. Scanning electron microscopy (SEM) is basically a type of electron microscope. The (SEM) study has been carried out by Hitachi (S-4160). The optical transmittance and absorbance spectrum of thin films of pure strontium titanium oxide (SrTiO₃) and doped by Boron(B) were measured by using an Ultraviolet-Visible Spectrophotometer. The Specifications of this device Model English industry (UV-2601) Spectrophotometer in wavelength range between (200-1100) nm.

Hall effect measurements, the HMS-3000 Hall Measurement System is a complete system for measuring the resistivity, carrier concentration, and mobility of semiconductors. At both 300K and 77K

(room temperature and liquid nitrogen temperature). The systems can be used to characterize various materials including semiconductors and compound semiconductors (N Type & P Type). Simple operation and speedy data results, simplicity and accuracy, 5 Stage current ranges reduce the allowance error to a minimum. The deposition parameters of Strontium titanate thin films as shown in Table 1.

Table 1. Deposition coefficient of Strontium titanate (SrTiO₃) thin films

Deposition coefficient	Value
SrCl ₂ , TiCl ₃ solution concentration substrate	0.1 M
Temperature (°C)	400°C
Nozzle to substrate distance	10 cm
Solvent	Distilled water and ethanol
Deposition time	60 minutes
Solution flow rate	1.5 ml/min
Spray time during each cycle	5 min
Ultrasonic frequency	1.5 M Hz
Dimeter of the nozzle	1 Cm

The weight is measured via an electrical balance sensitive four digits (10⁻⁴g). Eq. 1 was used for calculating the masses as shown in Table 2.

$$M = \frac{W_t}{M_{Wt} \cdot V} \times 1000 \quad (1)$$

Where: *M*: Concentration of molarities (mole/liter).

W_t : Weight of mass

M_{Wt}: Molecular weight mass

V: Volume of distilled water (ml).

Table 2. Weights of chemical composites of Sr_{1-x}B_xTiO₃ with difference molar ratio.

Doping Ratio x	Perovskite composite's	SrCl ₂ (m.mol)	H ₃ BO ₃ (m.mol)	TiCl ₃ (m.mol)
SrTiO ₃		2	0	2
Sr _{0.98} B _{0.02} TiO ₃		1.96	0.04	2
Sr _{0.96} B _{0.04} TiO ₃		1.92	0.08	2
Sr _{0.94} B _{0.06} TiO ₃		1.88	0.12	2
Sr _{0.92} B _{0.08} TiO ₃		1.84	0.16	2

RESULTS AND DISCUSSION

Structural Properties

X-ray diffraction (Shimadzu-6000, Cu K α radiation ($\lambda=1.54$ Å) was used to determine the crystallographic structure of SrTiO₃ and Sr_{1-x}B_xTiO₃ films prepared by the AACVD technique. It is can be noticed that all samples of pure SrTiO₃

and Sr_{1-x}B_xTiO₃ with a doping ratio (X = 2, 4, 6 and 0.8)% a single phase which was the cube structural, Space group Pm-3m with lattice constant a=3.96 Å, for pure SrTiO₃ corresponded to the crystalline planes (100), (110), (111), (200), (210) and (211) at reflections positions ($2\theta = 22.75, 32.39, 39.95, 46.46, 52.34$ and 57.78) respectively for Sr_{1-x}B_xTiO₃ corresponded to the crystalline planes (100), (110), (111) and (200) at reflections positions ($2\theta=22.84, 32.55, 40.02$ and 46.54) respectively, because prefer in orientation in (100), (110), (111) and (200) and reduced in (210) and (211) as following in Figure 1.

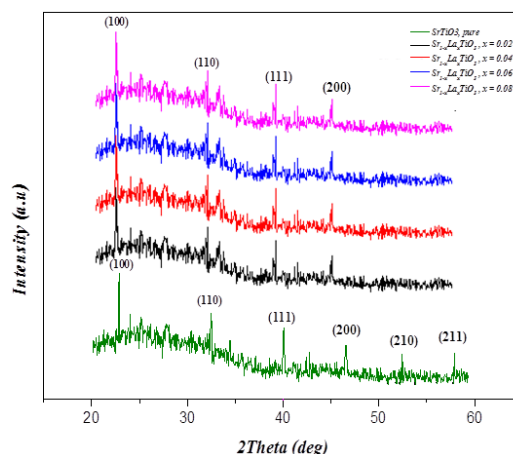


Figure 1. XRD patterns of. Sr_{1-x}B_xTiO₃ thin films at doping ratio (0.02 ≤ x ≤ 0.08).

From Scherer formula can calculated the crystallite size from Eq. (2), that the Boron atoms do not significantly affect the crystalline structure of pure SrTiO₃, but there was a slight decrease in the crystallite size with different doping ratios because these impurities work to force themselves in between the regular lattice sites, i.e. between the locations of the original atoms of the host crystal, due to the characteristics of atoms of this type of impurity from they have small atomic radii when compared to the interatomic distances for the host crystal [13, 14] as shown in Table 3.

The Crystallite size *D* can be calculate by Scherer formula Eq. 2.

$$D = \frac{k\lambda}{\beta_D \cos(\theta)} \quad (2)$$

Where: $k = 2 \sqrt{\frac{\ln(2)}{\pi}} = 0.94$ called (Scherer's constant), λ is the wavelength of incident X-ray radiation, β_D is the intrinsic Full Width at Half Maximum (FWHM) of the peak, and θ is the

Bragg's diffraction angle of the respective XRD peak.

Table 3. structural parameters of thin films samples of SrTiO₃ and Sr_{1-x}B_xTiO₃ at $x = (0.02 \leq x \leq 0.08)$.

Doping ratio (x)	Space group	A (A°)	Crystalline size of XRD (nm)
0.00	pm-3m	3.960	25
0.02	pm-3m	3.905	24
0.04	pm-3m	3.905	22
0.06	pm-3m	3.907	23
0.08	pm-3m	3.907	20

Figure 2 shows the surface morphology of deposited of pure SrTiO₃ and Sr_{1-x}B_xTiO₃ thin films which have been investigated by scanning electron microscopy (SEM). The test was measured at 200 kx magnification with 10 kV applied high voltage and 200 nm, of scale bars measured. Whereas Figure 2 depicts a thin film sample of pure SrTiO₃ and Sr_{1-x}B_xTiO₃, at an impurity ratio (2, 4, 6 and 8). The improvement in crystallization due to the increased in the regular periodic arrangement of the atoms in the crystal lattice [14]. The measurements were done with the same conditions for all the samples as shown in Figure 2.

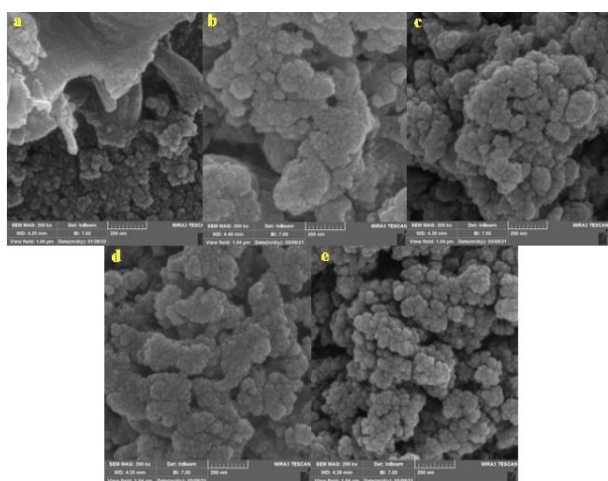


Figure 2. SEM images of Sr_{1-x}B_xTiO₃, (X=0 -8)% Thin films With B impurity ratios: a =pure, b=2%, c=4%, d= 6% and e=8%.

This roughness is increased with increase doping ratio by (B), this can be explained by the occurrence of crystal growth of grains perpendicular to the surface as shown in Table 4.

Table 4. Parameters of the structural properties of SrTiO₃ and Sr_{1-x}B_xTiO₃ at variation impurities.

Doping ratio (x) (RMS) nm Average	RMS (nm)	Roughness (nm)
0	41.07	27.76
0.02	92.54	72.84
0.04	105.05	86.05
0.06	123.30	101.30
0.08	164.87	127.72

Optical Properties

The transmittance spectrum (T%) is displayed according to Eq. 3 [15-17].

$$T = \exp^{-2.303A} \quad (3)$$

Where T is the transmittance, A is the absorbance. The transmittance spectrum is characterized by the opposite behavior of the absorbance spectrum, as shown in Figure 3 transmittance spectrum as a function of the wavelength of SrTiO₃ and Sr_{1-x}B_xTiO₃ thin films at doping ratios (X = 2, 4, 6 and 0.8) % at spectrum range (300-900) nm, the transmittance generally increases with the increase in the wavelength of radiation, at wavelengths with low energies. Observed a gradual decrease in the transmittance spectrum of pure SrTiO₃ thin films as shown in Figure 3. Gradual increase in the percentage of impurity taken, because of the impurity atoms and the accompanying composition local levels within the forbidden energy gap between the valence and conduction bands, and thus increase in absorbency and decrease in permeability.

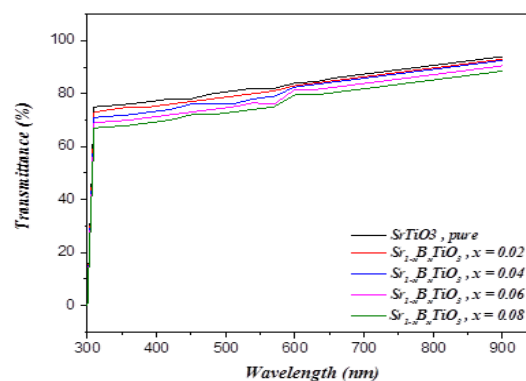


Figure 3. transmittance is a function of the wavelength of the for SrTiO₃ and Sr_{1-x}B_xTiO₃ thin films at doping ratios ($0.02 \leq x \leq 0.08$).

The absorbance spectra of the SrTiO₃ and Sr_{1-x}B_xTiO₃ thin films at doping ratios (X=2, 4, 6 and 0.8) % are shown in Figure 4. It has been found that the absorbance decreases slowly at spectrum rate (300-900) nm i.e. in the visible region. In the UV region the absorbance. The absorbance has been found to increase with increasing of Boron doped and it is maximum for 8% of B due to

increases of roughness and grain boundaries [18,19].

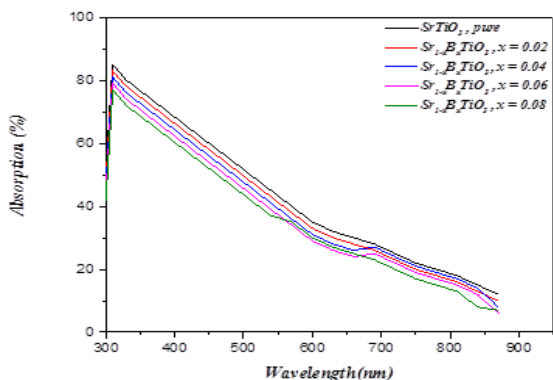


Figure 4. The absorption is a function of the wavelength of the for SrTiO₃ and Sr_{1-x}B_xTiO₃ thin films at doping ratios (0.02 ≤ x ≤ 0.08).

We note that the absorption coefficient increases with the increase of the doping ratio of SrTiO₃:La (it is inversely proportional to the transmittance) [19]. From: Figure 5 between $(\alpha h\nu)^2$ and $(h\nu)$ in eV, the direct bandgap was determined. A straight line is obtained that gives the value of the direct band gap. The energy band gap (E_g) can be calculated using the Eq. 4 [16], [20].

$$\alpha h\nu = A(h\nu - E_g)^r \quad (4)$$

Where α is the absorption coefficient, $h\nu$ is the photon energy, E_g is the optical band gap, A is a constant.

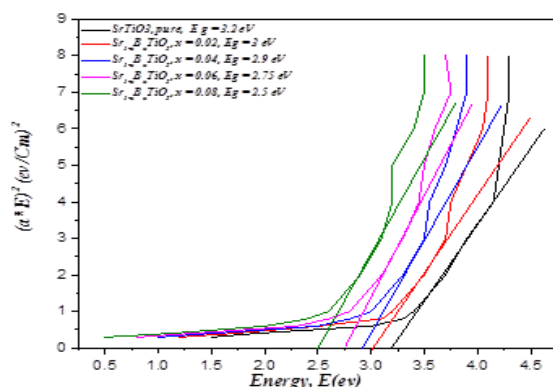


Figure 5. Optical energy gap of the SrTiO₃ and Sr_{1-x}B_xTiO₃ thin films at doping ratios (0.02 ≤ x ≤ 0.08).

The change due to the formation of local levels as a result of the doping process. doping B causes a decrease in the band gap energy. From Figure 5 the energy band gap (E_g) is decreased from 3.2 eV to 2.5 eV as the Eq. 4, which indicates that the doping process has led to the emergence of localized levels

in the region confined by the valence and conduction bands, led to a reduction in the photon energy required for direct electronic transitions to occur, which it makes the transfer of electrons from the valence band to the conduction band easier and this value agrees with the results of the researchers [21, 22].

Hall Effect Measurement

It this Hall effect is a result of the phenomenon whereby a magnetic field applied perpendicular to the direction of motion of a charged particle exerts a force on the particle perpendicular to both the magnetic field and the particle motion directions. Electrons or holes move in one direction in response to an externally applied electric field. The magnetic field is forced in a perpendicular direction. The force exerted on the charge carriers will deflect them in the direction of holes (positively charged carriers) and electrons (negatively charged carriers) in the other direction [23-25]. Have been measured variation of carrier concentration (n) and Hall mobility (μ_H) of SrTiO₃ and Sr_{1-x}B_xTiO₃ thin films as the function of B with different doping ratio (2, 4, 6 and 8)%, as shown in the Figure 6.

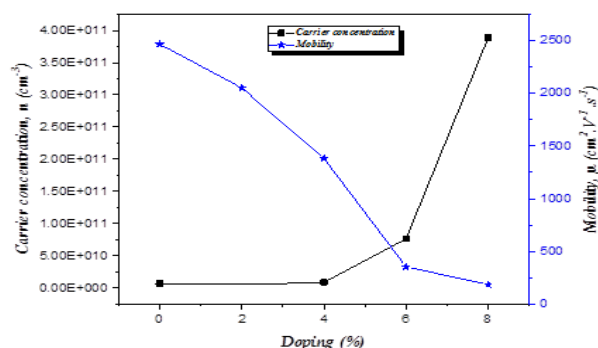


Figure 6. Variation of carrier doping concentration and Hall mobility of SrTiO and Sr_{1-x}B_xTiO₃ thin films with doping ratios (0.02 ≤ x ≤ 0.08).

Found the carriers concentration of charge are holes, p-type of Sr_{1-x}B_xTiO₃ thin films at doping ratio (x=2, 4, 6 and 8)%, it is seen that the carriers concentration are increased from $(6.776 \times 10^9 - 3.888 \times 10^{11}) \text{ cm}^{-3}$ as the B content are increasing at x=(0.00- 0.08). The increasing is attributed to increase the charge carrier [26-28]. The carrier concentration (n) is related to the Hall coefficient (RH) as expressed by the Eq. 5 [29], Hall mobility (μ_H) calculated simply from the Eq. 6 [30].

$$R_H = \frac{1}{nvev} \quad (5)$$

Where: R_H is the Hall coefficient, n is the concentration of charge and e is the carrier of charge. The Hall mobility of electrons (μ_H) is:

$$\mu_H = \frac{\sigma}{nvev} \quad (6)$$

or using the equation:

$$\mu_H = |R_H| \sigma \quad (7)$$

The carrier mobility decreases at ($2.467 \times 10^3 - 1.849 \times 10^2$) ($\text{cm}^2/\text{V.s}$) at the doping ratio (0-0.08) and the Hall coefficient (RH) decreases also due to increasing of carrier concentrations according to the Eq. 5 so that the Hall mobility decreases Eq. 6 [31, 32].

CONCLUSIONS

SrTiO₃ pure and doped SrTiO₃: B thin films were prepared via AACVD technique, the advantage of this method is that it is inexpensive and easy to use. A homogeneous membrane can be obtained with high adhesion. It is also possible to deposit at different deposition angles and on different surfaces with the same efficiency in this way. The optical band gap decreased at (3.2-2.5) eV with increased doping ratio. We should remind that the resistivity of these films is low; therefore, these samples can be applied as an absorber layer in the fabrication of solar cells. The conductivity of the thin film is increased at height doping ratio therefore can be used in the sensors application.

Disclosure and conflict of interest: The authors declare that they have no conflicts of interest.

REFERENCES

- [1] G. Canu and V. Buscaglia, "Hydrothermal synthesis of strontium titanate: Thermodynamic considerations, morphology control and crystallisation mechanisms," *CrystEngComm*, vol. 19, no. 28, pp. 3867-3891, 2017. <https://doi.org/10.1039/C7CE00834A>
- [2] B. J. Huang, C. J. Chin, and C. L. Duang, "Design method of thermoelectric cooler," *Int. J. Refrig.*, vol. 23, no. 3, pp. 208-218, 2000. [https://doi.org/10.1016/S0140-7007\(99\)00046-8](https://doi.org/10.1016/S0140-7007(99)00046-8)
- [3] J. Hwang, R. R. Rao, L. Giordano, Y. Katayama, Y. Yu, and Y. Shao-Horn, "Perovskites in catalysis and electrocatalysis," *Science (80-.)*, vol. 358, no. 6364, pp. 751-756, 2017. <https://doi.org/10.1126/science.aam7092>
- [4] J. W. Fergus, "Oxide materials for high temperature thermoelectric energy conversion," *J. Eur. Ceram. Soc.*, vol. 32, no. 3, pp. 525-540, 2012. <https://doi.org/10.1016/j.jeurceramsoc.2011.10.007>
- [5] R. Molinari, C. Lavorato, and P. Argurio, "Visible-light photocatalysts and their perspectives for building photocatalytic membrane reactors for various liquid phase chemical conversions," *Catalysts*, vol. 10, no. 11, pp. 1-38, 2020. <https://doi.org/10.3390/catal10111334>
- [6] S. Xiao, M. Yao, W. Gao, Z. Su, and X. Yao, "Significantly enhanced dielectric constant and breakdown strength in crystalline/amorphous core-shell structured SrTiO₃ nanocomposite thick films," *J. Alloys Compd.*, vol. 762, pp. 370-377, 2018. <https://doi.org/10.1016/j.jallcom.2018.05.221>
- [7] J. Lu, S. Schmidt, Y. W. Ok, S. P. Keane, and S. Stemmer, "Contributions to the dielectric losses of textured SrTiO₃ thin films with Pt electrodes," *J. Appl. Phys.*, vol. 98, no. 5, 2005. <https://doi.org/10.1063/1.2034649>
- [8] C. E. Ekuma, M. Jarrell, J. Moreno, and D. Bagayoko, "First principle electronic, structural, elastic, and optical properties of strontium titanate," *AIP Adv.*, vol. 2, no. 1, 2012. <https://doi.org/10.1063/1.3700433>
- [9] Y. Shan et al., "Thickness-dependent optical properties of yttrium fluoride ultrathin films in the visible band," *Opt. Mater. Express*, vol. 10, no. 12, p. 3306, 2020. <https://doi.org/10.1364/OME.398536>
- [10] L. Li et al., "Bilayered Hybrid Perovskite Ferroelectric with Giant Two-Photon Absorption," *J. Am. Chem. Soc.*, vol. 140, no. 22, pp. 6806-6809, 2018. <https://doi.org/10.1021/jacs.8b04014>
- [11] C. Lee, J. Destry, and J. L. Brebner, "Optical absorption and transport in semiconducting SrTiO₃," *Phys. Rev. B*, vol. 11, no. 6, pp. 2299-2310, 1975. <https://doi.org/10.1103/PhysRevB.11.2299>
- [12] L. Kovács and G. Corradi, "New trends in lithium niobate: From bulk to nanocrystals," *Crystals*, vol. 11, no. 11, 2021. <https://doi.org/10.3390/cryst11111356>
- [13] Z. Li, W. Zhou, X. Su, F. Luo, Y. Huang, and C. Wang, "Effect of boron doping on microwave dielectric properties of SiC powder synthesized by combustion synthesis," *J. Alloys Compd.*, vol. 509, no. 3, pp. 973-976, 2011. <https://doi.org/10.1016/j.jallcom.2010.08.156>
- [14] S. De Almeida-Didry, C. Autret, A. Lucas, F. Paireau, and F. Gervais, "Comparison of colossal permittivity of CaCu₃Ti₄O₁₂ with commercial grain boundary barrier layer capacitor," *Solid State Sci.*, vol. 96, no. July, p. 105943, 2019. <https://doi.org/10.1016/j.solidstatesciences.2019.105943>
- [15] N. H. Harb, "The structure and optical properties of Ag doped cdo thin film prepared by pulse laser deposition (PLD)," *Baghdad Sci. J.*, vol. 15, no. 3, pp. 300-303, 2018. <https://doi.org/10.21123/bsj.15.3.314-323>
- [16] B. S. Journal, "The Effect of annealing temperature on the optical properties of (Cu₂S)_{100-x}(SnS₂)_x thin films," *Baghdad Sci. J.*, vol. 11, no. 2, pp. 641-651, 2014. <https://doi.org/10.21123/bsj.11.2.641-651>

- [17] G. Patwari, P. K. Kalita, and R. Singha, "Structural and optoelectronic properties of glucose capped Al and Cu doped ZnO nanostructures," *Mater. Sci. Pol.*, vol. 34, no. 1, pp. 69-78, 2016.
<https://doi.org/10.1515/msp-2016-0030>
- [18] Y. M. Abdul-Hussein, H. J. Ali, L. A. Latif, M. A. Abdulsattar, and H. M. Fadhel, "Preparation of Al-doped NiO thin films by spray pyrolysis technique for CO gas sensing," *J. Adv. Pharm. Educ. Res.*, vol. 9, no. 3, pp. 1-6, 2019.
- [19] M. Choi et al., "Structural, optical, and electrical properties of strained La-doped SrTiO₃ films," *J. Appl. Phys.*, vol. 116, no. 4, 2014.
<https://doi.org/10.1063/1.4891225>
- [20] H. J. Mohamad, Y. M. Abdul-Hussein, and U. A. S. Al-Jarah, "The structural, optical, and morphological properties of NiO-Cu prepared by spray pyrolysis technique," *Microw. Opt. Technol. Lett.*, vol. 62, no. 11, pp. 3519-3526, 2020.
<https://doi.org/10.1002/mop.32500>
- [21] H. Zeng, M. Wu, H. Q. Wang, J. C. Zheng, and J. Kang, "Tuning the magnetism in boron-doped strontium titanate," *Materials (Basel)*, vol. 13, no. 24, pp. 1-14, 2020.
<https://doi.org/10.3390/ma13245686>
- [22] A. B. Posadas, C. Lin, A. A. Demkov, and S. Zollner, "Bandgap engineering in perovskite oxides: Al-doped SrTiO₃," *Appl. Phys. Lett.*, vol. 103, no. 14, pp. 1-5, 2013.
<https://doi.org/10.1063/1.4824023>
- [23] J. Liu, H. Yang, Z. Ma, K. Chen, X. Huang, and K. Wang, "HfO₂/TiO₂ bilayer structure memristor with linear conductance tuning for high density memory and neuromorphic computing," *J. Appl. Phys.*, vol. 128, no. 18, 2020.
<https://doi.org/10.1063/5.0024668>
- [24] H. T. Yi, Y. N. Gartstein, and V. Podzorov, "Charge carrier coherence and Hall effect in organic semiconductors," *Sci. Rep.*, vol. 6, no. February, pp. 1-11, 2016.
<https://doi.org/10.1038/srep23650>
- [25] Q. Zhang et al., "Realizing a thermoelectric conversion efficiency of 12% in bismuth telluride/skutterudite segmented modules through full-parameter optimization and energy-loss minimized integration," *Energy Environ. Sci.*, vol. 10, no. 4, pp. 956-963, 2017.
<https://doi.org/10.1039/C7EE00447H>
- [26] W. Cai et al., "Sulfur-tolerant Fe-doped La_{0.3}Sr_{0.7}TiO₃ perovskite as anode of direct carbon solid oxide fuel cells," *Energy*, vol. 211, p. 118958, 2020.
<https://doi.org/10.1016/j.energy.2020.118958>
- [27] M. Ghasemifard, M. E. Abrishami, and M. Iziy, "Effect of different dopants Ba and Ag on the properties of SrTiO₃ nanopowders," *Results Phys.*, vol. 5, pp. 309-313, 2015.
<https://doi.org/10.1016/j.rinp.2015.10.005>
- [28] R. Li, C. Zhang, J. Liu, J. Zhou, and L. Xu, "Study on the electrical conductivity of In-doped SrTiO₃ with B-site deficiency prepared by sol-gel method," *Mater. Res. Express*, vol. 6, no. 10, pp. 0-6, 2019.
<https://doi.org/10.1088/2053-1591/ab3fe5>
- [29] S. Entler et al., "Ceramic-chromium hall sensors for environments with high temperatures and neutron radiation," *Sensors (Switzerland)*, vol. 21, no. 3, pp. 1-12, 2021.
<https://doi.org/10.3390/s21030721>
- [30] T. V. Vimalkumar, "Highly conductive and transparent ZnO thin film using Chemical Spray Pyrolysis technique: Effect of doping and deposition parameters," no. August, p. 8, 2011.
- [31] S. H. Park et al., "Modeling the electrical resistivity of polymer composites with segregated structures," *Nat. Commun.*, vol. 10, no. 1, pp. 1-11, 2019.
<https://doi.org/10.1038/s41467-019-10514-4>
- [32] I. Kamińska and A. Szwed, "A thermodynamically consistent model of quasibrittle elastic damaged materials based on a novel helmholtz potential and dissipation function," *Materials (Basel)*, vol. 14, no. 21, 2021.
<https://doi.org/10.3390/ma14216323>

How to Cite

Y. M. . Abdul-Hussein, R. K. . Hussain, and M. K. . Khalaf, "Aerosol-Assisted Chemical Vapor Deposition (AACVD) Technique of SrTiO₃: B Thin Films and Study the Structural and Optical Properties and Hall Effect Measurements", *Al-Mustansiriyah Journal of Science*, vol. 33, no. 4, pp. 124–130, Dec. 2022.